Journal of Materials Chemistry

Cite this: J. Mater. Chem., 2011, 21, 10426

www.rsc.org/materials

PAPER

Protic ionic liquid and ionic melts prepared from methanesulfonic acid and 1*H*-1,2,4-triazole as high temperature PEMFC electrolytes†

Jiangshui Luo,[abc] Jin Hu,[a] Wolfgang Saak,[c] Rüdiger Beckhaus,[c] Gunther Wittstock,[c] Ivo F. J. Vankelecom,*[b] Carsten Agert[a] and Olaf Conrad*[ad]

Received 9th December 2010, Accepted 1st March 2011
DOI: 10.1039/c0jm04306k

Protic ionic liquid and ionic melts were prepared from the combination of methanesulfonic acid (CH_3SO_3H) and 1*H*-1,2,4-triazole ($C_2H_3N_3$) at various molar ratios. The thermal properties, crystal structure, acid–base interactions, ionic conductivity, proton conduction behavior and electrochemical stability of the system were studied. The equimolar composition, 1,2,4-triazolium methanesulfonate ($C_2H_4N_3^+ \cdot CH_3SO_3^-$ (**1**)), was a proton transfer salt with a melting point of around 134 °C. Single crystal and powder XRD data, as well as TGA results, revealed that the base-rich region was a mixture of **1** and 1*H*-1,2,4-triazole. Infrared analysis and single crystal data suggested that the $C_2H_3N_3$–CH_3SO_3H system exists in a strongly hydrogen-bonded network. Systematic investigation of the ionic conductivity showed that the ionic conductivity reached local maxima at the compositions of $[C_2H_3N_3]/[CH_3SO_3H]$ = 10/90 and 80/20, respectively, while it exhibited a local minimum at the equimolar composition. The temperature dependence of the ionic conductivity was found to obey the Vogel–Fulcher–Tamman (VFT) equation. The fitting of the conductivity data to the VFT equation showed that the carrier ion concentration *versus* the mole fraction of 1*H*-1,2,4-triazole exhibited a volcano shape. In addition, the $C_2H_3N_3$–CH_3SO_3H system showed adequate electrochemical stability under PEMFC conditions as measured by linear sweep voltammetry. The relatively high ionic conductivity, wide electrochemical window and good thermal stability demonstrated that the $C_2H_3N_3$–CH_3SO_3H system is a suitable candidate for high temperature PEMFC electrolytes.

1 Introduction

High temperature polymer electrolyte membrane fuel cells (PEMFCs) operating at temperatures of 100–200 °C can yield significant benefits, such as enhanced electrochemical reaction rates, simpler system and better CO tolerance.[1] However, they face one major challenge: the lack of suitable proton exchange membrane materials with little dependence on the humidity at high temperature.[2] Even Nafion®, the state-of-the-art polymer membrane material, suffers a drastic decrease of the proton conductivity at low relative humidity.[3]

Recently, protic ionic liquids (PILs) have been explored as a possible approach to develop non-aqueous proton-conducting electrolytes.[4–19] PILs are formed by proton transfer between Brønsted acids and bases.[4] They exhibit low volatility and relatively high ionic conductivity.[5] Often they are also characterized by non-flammability and good thermal as well as electrochemical stability, making them promising electrolyte materials for high temperature PEMFCs.[4–10] Considerable efforts have been being devoted to the incorporation of PILs in polymer matrices such as thermoplastic polymers,[6] sulfonated polyimides (SPIs)[7] or Nafion® membranes,[8] the polymerization of monomers in PILs,[9] and the fixation of the cation or anion structure in the polymer segments.[10–14] For example, Watanabe *et al.*[7a] used the solution casting method to fabricate composite membranes using SPIs and diethylmethylammonium trifluoromethanesulfonate. The composite membranes exhibited good thermal stability, high ionic conductivity, and mechanical strength and gas permeation comparable to those of hydrated Nafion. In addition, H_2/O_2 fuel cells successfully operated using the composite membranes at

[a]*NEXT ENERGY EWE-Forschungszentrum für Energietechnologie e.V., Carl-von-Ossietzky-Str. 15, D-26129 Oldenburg, Germany*
[b]*Centre for Surface Chemistry and Catalysis, Faculty of Bioscience Engineering, Katholieke Universiteit Leuven, Kasteelpark Arenberg 23, Box 2461, B-3001 Leuven, Belgium. E-mail: ivo.vankelecom@biw.kuleuven.be; Fax: +32 16 321998; Tel: +32 16 321594*
[c]*Institut für Reine und Angewandte Chemie, Carl von Ossietzky Universität Oldenburg, D-26111 Oldenburg, Germany*
[d]*HySA/Catalysis, Department of Chemical Engineering, University of Cape Town, Private Bag X3 Rondebosch, 7701 Cape Town, South Africa. E-mail: olaf.conrad@uct.ac.za; Tel: +27 21650 4366*

† Electronic supplementary information (ESI) available: Crystallographic information file (CIF) for 1,2,4-triazolium methanesulfonate, torsion angles, density of the liquid compositions in the acid-rich region, TG curves in O_2 atmosphere and X-ray thermodiffraction patterns. CCDC reference numbers 804598. For ESI and crystallographic data in CIF or other electronic format see DOI: 10.1039/c0jm04306k

temperatures from 30 to 140 °C under non-humidified conditions, and a current density of 250 mA cm^{-2} was achieved at 120 °C.[7a] Iojoiu *et al.* reported that the half-neutralized diamine based PILs were found to reinforce markedly the Nafion based membranes through physical cross-linking.[8b] Besides, PIL-based membranes, prepared by polymerization of microemulsions consisting of surfactant-stabilized PIL nanodomains dispersed in a polymerizable oil, showed a conductivity of up to the order of 1×10^{-1} S cm^{-1} at 160 °C under non-humidifying conditions, due to the well-connected PIL nanochannels preserved in the membrane.[9a] All these demonstrated that PILs and their composite membranes are particularly advantageous for high temperature PEMFCs operating under non-humidified conditions.

Therefore, for a broad development of PIL-based membranes, it is necessary to systematically study Brønsted acid–base PIL systems, which have been carried out to a limited extend.[13,18–22] Kreuer *et al.*[20] observed that the ionic conductivity of the H_2SO_4–imidazole system is remarkably changed with the change of imidazole content. They believed that the addition of basic molecules such as imidazole to oxoacids increased the number of defect protons in the system and therefore increased the proton conductivity of the system. Watanabe *et al.*[18,19] introduced the Brønsted acid–base ionic liquid system as a new candidate for fuel cell electrolytes to operate under anhydrous conditions and at elevated temperature. They prepared protic ionic liquid and ionic melts by combination of bis(trifluoromethanesulfonyl) imide (HTFSI) and benzimidazole (BIm) at various molar ratios.[19] They showed that the equimolar salt and base-rich BIm–HTFSI melts can serve as H_2/O_2 fuel cell electrolytes under non-humidified conditions and at temperatures higher than 100 °C. However, PILs prepared from HTFSI tend to exhibit high overpotentials for oxygen reduction reaction.[15a,b,18,19] In addition, the electrochemical stability of imidazole appears to be inadequate for fuel cell applications.[23]

It is reported that protic ionic liquids prepared from oxoacids (*e.g.* CF_3SO_3H) tend to exhibit low overpotentials for H_2 oxidation and O_2 reduction.[15b,e] Among the oxoacids, methanesulfonic acid (CH_3SO_3H) is a strong acid ($pK_a = -1.92$).[24] It is a halogen-free, low toxicity, relatively stable and readily biodegradable compound, making it an environmentally advantageous electrolyte.[25] 1*H*-1,2,4-Triazole has a high boiling point (260 °C[26]) and is a superior anhydrous proton transfer agent compared to imidazole.[13,27] It has no drastic poisoning effect on platinum electrodes and is electrochemically stable under fuel cell conditions.[13] These prospective advantages have prompted us to study the protic ionic liquid and ionic melts prepared from methanesulfonic acid and 1*H*-1,2,4-triazole under anhydrous conditions as potential electrolytes for high temperature PEMFCs. In this paper, the thermal properties, crystalline structure, acid–base interactions, ionic conductivity, proton conduction behavior and electrochemical stability of the system were systematically explored.

2 Experimental

2.1 Materials

Methanesulfonic acid (CH_3SO_3H, Sigma-Aldrich, ≥99.5%) and 1*H*-1,2,4-triazole ($C_2H_3N_3$, Acros Organics, 99.5%) were used as received. Appropriate amounts of CH_3SO_3H and $C_2H_3N_3$, maintaining defined molar ratios (*i.e.* $[C_2H_3N_3]/[CH_3SO_3H]$ = 0/100, 5/95, …, 90/10, 95/5, 100/0), were mixed and heated above the respective melting points to prepare the ionic liquid and ionic melts. The as-prepared samples can be divided into equimolar composition ($[C_2H_3N_3]/[CH_3SO_3H] = 50/50$) and acid-rich and base-rich materials (*i.e.* the ionic melts). Most of the compositions in the acid-rich region were liquid, while the equimolar and base-rich compositions were solid at room temperature. All samples were handled and stored in a UniLab glove box (MBRAUN) with pure N_2 atmosphere (water content <0.1 ppm).

2.2 Water content and anion impurities

A coulometric Karl Fischer moisture titrator (Model CA-200, Mitsubishi Chemical Analytech) was used to determine the water content of the compositions.

The $CH_3SO_3^-$ concentration and anion impurities such as halide and sulfate ions were determined by ion chromatography. The ion chromatographic analysis was performed at 30 °C using a Metrohm 850 Professional IC (Metrohm, Herisau, Switzerland) with ProfIC-1-Anion system, equipped with a Metrosep A Supp 5 analytical column (150 × 4.0 mm). The anions were determined by suppressed conductivity detection. The injection volume was 20 μL. Data were collected using a Metrohm 850 data acquisition system interfaced to a computer running MagIC Net 2.0 software. Deionized water from Millipore Simplicity UV System (Molsheim, France) with a specific resistivity of 18.2 MΩ cm at 25 °C was used for all eluent, sample, and standard preparations. The equimolar composition was 1000 times diluted (*i.e.* mass fraction of sample is 0.1%) using deionized water. The eluent was 3.2 mmol L^{-1} Na_2CO_3 + 1.0 mmol L^{-1} $NaHCO_3$, and the suppressor regenerating solution was 0.1 mol L^{-1} H_2SO_4.[28] The flow rate of the eluent was 0.700 mL min^{-1}. For halide and sulfate determination, a certified multianion standard solution PRIMUS (Sigma-Aldrich) containing 10.0 mg kg^{-1} ± 0.2% of each F^-, Cl^-, Br^-, NO_3^-, SO_4^{2-} and PO_4^{3-} was used. For the measurement of the $CH_3SO_3^-$ concentration, 99.5% methanesulfonic acid was 10 000, 5000 and 2500 times diluted, respectively, to prepare three standard CH_3SO_3H solutions of different $CH_3SO_3^-$ concentrations. Since CH_3SO_3H is a strong monoacid, the $CH_3SO_3^-$ concentrations were calculated to be 98.5, 197 and 394 ppm, respectively. The values were further confirmed by pH titrations using TitroLine alpha plus (SI Analytics). The experimental pH values were 2.98, 2.68, and 2.39, respectively.

2.3 Thermal analysis

Differential thermal analysis (DTA) and thermal stability investigations for the samples were carried out on a thermogravimetry/differential thermal analyzer (TGA/SDTA 851ᵉ, Mettler Toledo) from room temperature to 450 °C at a heating rate of 10 K min^{-1} under a N_2 flow of 60 mL min^{-1} with covered Al_2O_3 pans. The sample weight was controlled to be between 12 and 15 mg. The melting points (T_m, onset of the endothermic peak) of the equimolar composition and 1*H*-1,2,4-triazole, as well as the eutectic temperature (T_e, onset of the endothermic

peak) and melting points (T_m, determined from the temperature of the related endothermic peak) of the base-rich compositions, were determined from DTA thermograms during the heating scans. The decomposition temperature, T_d, was determined from the temperature at 10% mass loss during heating scans from the room temperature by using thermogravimetric analysis (TGA). Additionally, TGA for an average sample weight of 15 mg heated at 1 K min^{-1} was performed on a thermogravimetric analyzer (TGA 4000, PerkinElmer) in a stream of N_2 (30 mL min^{-1}) with open Al_2O_3 pans. Calcium oxalate monohydrate ($CaC_2O_4 \cdot H_2O$) was used as the standard substance for calibration.

2.4 X-Ray diffraction

A single crystal of 1,2,4-triazolium methanesulfonate ($C_2H_4N_3^+ \cdot CH_3SO_3^-$ (**1**)) was isolated from the preparation of $[C_2H_3N_3]/[CH_3SO_3H] = 1/2$ composition, which was a mixture of liquid and solid at room temperature. Single crystal X-ray diffraction (XRD) data were recorded on a STOE IPDS diffractometer (Mo Kα radiation, $\lambda = 0.71073$ Å) at 153 K. The structure was solved with SHELXS-97 and then refined with SHELXL-97.[29] In addition, powder XRD measurements were performed for the $[C_2H_3N_3]/[CH_3SO_3H]$ = 50/50, 75/25 and 100/0 compositions on a powder X-ray diffractometer (X'Pert PRO, PANalytical) using Cu Kα radiation (λ = 1.5406 Å) at room temperature.

2.5 Fourier transform infrared (FT-IR) spectra

The as-prepared samples were characterized by FT-IR. For the liquid compositions in the acid-rich region, the samples were measured as liquids between two NaCl windows against a NaCl background in the range of 4000–600 cm^{-1} using a Bruker Vertex 70 FT-IR spectrometer with 100 scans and at a spectral resolution of 4 cm^{-1}. After each measurement, the NaCl plates were cleaned with CH_2Cl_2 and then held in vacuum for 30 min to remove CH_2Cl_2. The IR spectra for equimolar composition and the base-rich compositions (all were solid) were recorded in the range of 4000–650 cm^{-1} on a PerkinElmer Spectrum 100 FT-IR spectrometer with universal ATR accessory (crystal: diamond/ZnSe) and were accumulated for 10 scans at a resolution of 4 cm^{-1}.

2.6 Ionic conductivity

The ionic conductivity of the ionic liquid and ionic melts was determined by the complex impedance method using a Solartron 1255B Frequency Response Analyzer combined with a Solartron 1287 Electrochemical Interface in the frequency range from 1 Hz to 1 MHz. ZPlot® and ZView™ (Scribner Associates) software was used to collect and analyze the data. The samples were filled in a dip-type glass cell heated in a silicon oil bath. The temperature was controlled at 10 K interval (±0.01 K) using a LAUDA Proline heating thermostat P5 from low temperature to high temperature. The samples were thermally equilibrated at each temperature for at least 40 min prior to the measurements with a Pt100 platinized conductivity cell (model 6.0908.11, Metrohm). The cell constant was calibrated each time with 0.01 mol L^{-1} KCl solution at 25 °C. The resistance was determined from the first real axis touchdown point in the Nyquist plot of the impedance data.[30] Each data were measured with at least two different samples of the same composition from different synthesis batches to ensure the reproducibility within 5% in absolute value.[31]

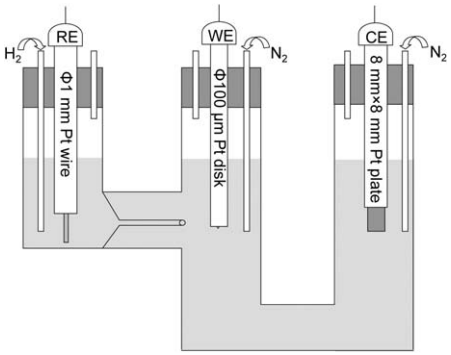

Fig. 1 Schematic diagram of the three-electrode system.

2.7 Linear sweep voltammograms

Linear sweep voltammograms (LSVs) were measured at 150 °C for different compositions with a three-electrode system shown in Fig. 1 at a scan rate of 2 mV s^{-1}. The working electrode (WE) was a 100 μm diameter Pt micro-disk electrode (no. 002009, BAS Inc.) and the counter electrode (CE) an 8 mm × 8 mm Pt plate (XM140, Radiometer Analytical). Both the WE and CE were in N_2 purged electrolyte. The reference electrode (RE) was a 1 mm diameter Pt wire (XM110, Radiometer Analytical) immersed in the testing composition with H_2 bubbling as a reversible hydrogen electrode (RHE), and was placed close to the WE *via* a Luggin capillary.[7a,15a] LSVs were performed with a Solartron 1287 Electrochemical Interface. CorrWare® and CorrView™ (Scribner Associates) software was used to collect and analyze the data.

3 Results and discussion

3.1 Water content and anion concentrations

The impurities of the as-prepared $C_2H_3N_3$–CH_3SO_3H samples include water, sulfate and halides. The water content was typically less than 2700 ppm. Ion chromatographic results showed that the chloride and sulfate contents of the equimolar composition were 16 and 80 ppm, respectively. No other halides were detected. The $CH_3SO_3^-$ ion concentration of the equimolar composition was obtained as 57.16%, which is very close to the calculated value of 57.29%, indicating the high accuracy of preparation of the ionic liquid and ionic melts.

3.2 Crystal structure

Crystal data. $C_3H_7N_3O_3S$, $M = 165.18$, monoclinic, $a = 5.4497(4)$ Å, $b = 7.4823(7)$ Å, $c = 16.7814(13)$ Å, $\beta = 95.212(8)°$, $U = 681.45(10)$ Å^3, $T = 153(2)$ K, space group $P2_1/c$ (no. 14), $Z = 4$, 7990 reflections measured, 1608 unique ($R_{int} = 0.0477$) which were used in all calculations. The final w$R(F^2)$ was 0.0574 (all data).

The molecular structure of **1** is shown in Fig. 2 in the form of Oak Ridge Thermal Ellipsoid Plot (ORTEP).[32] As has been

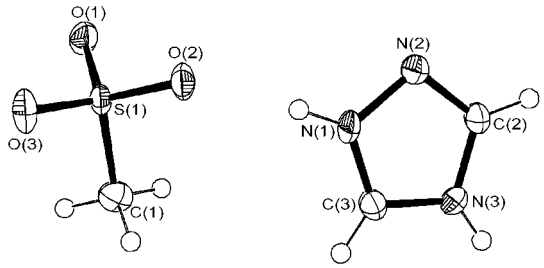

Fig. 2 ORTEP drawing of **1** with the atom-numbering scheme, showing 50% probability displacement ellipsoids. H atoms are drawn as spheres of arbitrary size.

Table 1 Selected bond lengths (Å) and bond angles (°) of **1**

N(1)–N(2)	1.3716(18)	C(3)–N(1)–N(2)	111.60(13)
N(1)–C(3)	1.304(2)	C(2)–N(2)–N(1)	103.16(13)
N(2)–C(2)	1.304(2)	C(3)–N(3)–C(2)	106.20(14)
N(3)–C(2)	1.356(2)	N(2)–C(2)–N(3)	111.81(14)
N(3)–C(3)	1.331(2)	N(1)–C(3)–N(3)	107.23(13)

pointed out by Drummond *et al.*,[33] the key properties that distinguish PILs from other ionic liquids are the proton transfer from the acid to the base, leading to the presence of proton-donor and proton-acceptor sites, which can be used to build up a hydrogen-bonded network. In this molecular structure, there is one ion pair in the asymmetric unit with one significant N–H···O hydrogen bond between the 1,2,4-triazolium cation and the methanesulfonate anion. The donor–acceptor (N(1)–O(2)) distance is 2.715(2) Å, which results in H···O length of 1.87(2) Å. The contact is well within the sum of the van der Waals radii ($r_H + r_O = 2.70$ Å).[34] The N–H···O angle of 175(2)° indicates the strongly directional rather than purely electrostatic interaction.

Table 1 shows the bond lengths and bond angles of 1,2,4-triazolium ring of **1**. The geometry of the 1,2,4-triazolium cation is comparable to the structure of 1*H*-1,2,4-triazole.[35] Particularly, the bond lengths and bond angles agree well with those of 1,2,4-triazolium chloride.[36] In this work, the longest C–N bond of the 1,2,4-triazolium ring, N(3)–C(2), is located opposite the atom N(1), while the shortest ones are N(1)–C(3) and N(2)–C(2), both of which are 1.304(2) Å long. The bond length of N(3)–C(3) is intermediate. The ring angles of the 1,2,4-triazolium cation range from 103.16(13)° to 111.81(14)°. In addition, from the torsion angles shown in Table S1† it is obvious that the 1,2,4-triazolium ring is essentially planar.

As can be seen in Fig. 3, the experimental powder XRD pattern of the bulk sample of equimolar composition at room temperature is well matched with that calculated from the single crystal data of **1** at 153 K, indicating that the equimolar composition should be the compound of **1**. Obviously, 1,2,4-triazolium methanesulfonate was formed at the equimolar composition according to the following equation:

$$C_2H_3N_3 + CH_3SO_3H \rightarrow \mathbf{1} \quad (1)$$

Fig. 4 shows that the powder XRD pattern of $[C_2H_3N_3]/[CH_3SO_3H] = 75/25$ was the combination of those of **1** and 1*H*-1,2,4-triazole, indicating that the crystalline fraction of the $C_2H_3N_3/CH_3SO_3H$ blend in the base-rich region was a mixture of **1** and 1*H*-1,2,4-triazole.

3.3 Thermal properties

The melting temperature, T_m, of the as-prepared $C_2H_3N_3$–CH_3SO_3H samples varied with composition. It was observed that the $C_2H_3N_3$–CH_3SO_3H mixtures formed homogeneous liquids above each T_m. The thermal properties for the base-rich compositions are listed in Table 2. For pure 1*H*-1,2,4-triazole, the measured average T_m was 121 °C, consistent with the literature value of 121 °C.[26] The equimolar composition had the highest T_m of 134 °C. Interestingly, as shown in Fig. S2†, the X-ray thermodiffraction patterns of **1** in Ar atmosphere indicated that **1** lost its crystallinity at around 129 °C. In addition, one eutectic composition with eutectic temperature $T_e = 66$ °C was found to fall within the compositions between $[C_2H_3N_3]/[CH_3SO_3H] = 70/30$ and 80/20.

The thermal decomposition (or evaporation) temperatures of the equimolar and base-rich compositions as a function of mole fraction of 1*H*-1,2,4-triazole are shown in Fig. 5a. Resembling the thermal behavior of some previously reported Brønsted

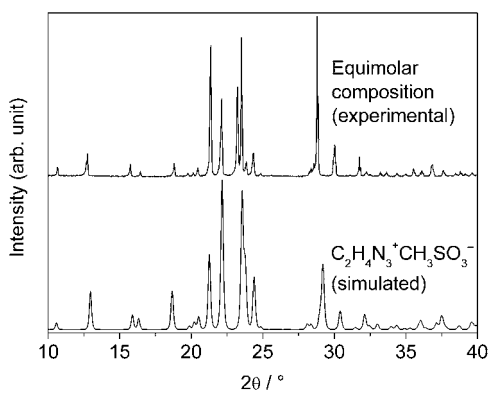

Fig. 3 Comparison of the powder XRD pattern of the bulk sample of equimolar composition at room temperature (top) with that simulated from the single crystal data of **1** at 153 K (bottom).

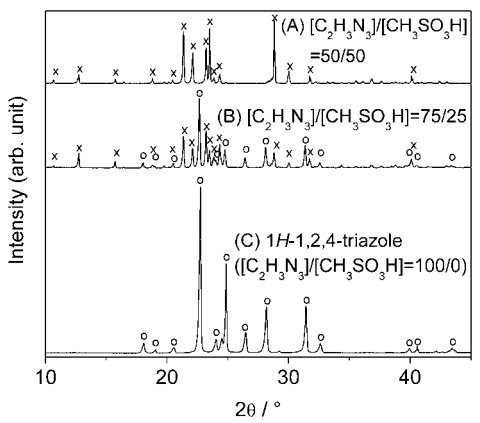

Fig. 4 Comparison of powder XRD patterns of **1** (A), $[C_2H_3N_3]/[CH_3SO_3H] = 75/25$ (B), and 1*H*-1,2,4-triazole (C). The peaks corresponding to A and C are marked with "x" and "o", respectively.

Table 2 Thermal properties for base-rich region of $C_2H_3N_3$–CH_3SO_3H system

$[C_2H_3N_3]/[CH_3SO_3H]$	T_e/°C	T_m/°C
50/50		134
55/45	65	129
60/40	66	118
65/35	66	103
70/30[a]	68	
75/25[a]	66	
80/20[a]	66	
85/15	65	96
90/10	64	110
95/5	64	114
100/0		121

[a] T_m was observed to be lower than 90 °C but not available from DTA curve due to overlapping peaks.

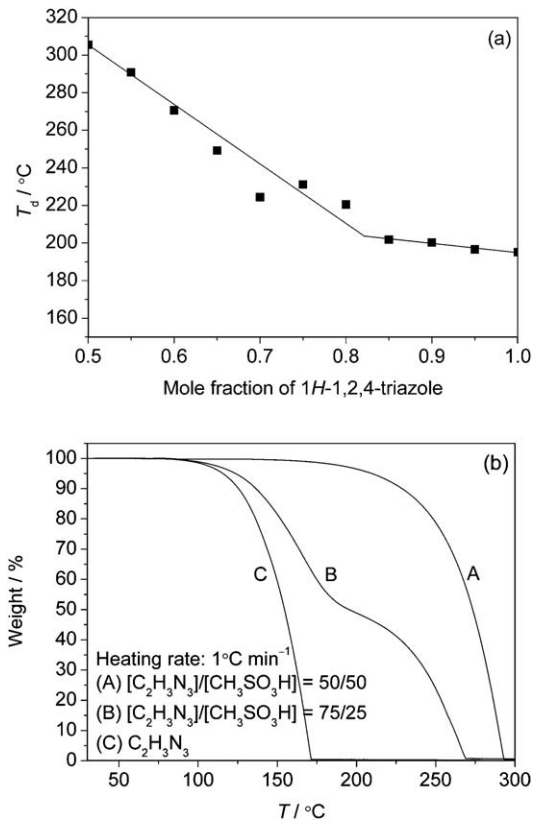

Fig. 5 (a) Decomposition temperatures (T_d) *versus* mole fraction of $C_2H_3N_3$ in $C_2H_3N_3$–CH_3SO_3H system, determined by TGA, heated at 10 K min^{-1} with covered Al_2O_3 pans; (b) TG curves of $C_2H_3N_3$ (A), $[C_2H_3N_3]/[CH_3SO_3H]$ = 75/25 (B) and $[C_2H_3N_3]/[CH_3SO_3H]$ = 50/50 (C), heated at 1 K min^{-1} with open Al_2O_3 pans.

acid–base ionic liquid and ionic melts,[18,19] T_d reached a maximum for the equimolar composition. The thermal stability decreases rapidly in the 1*H*-1,2,4-triazole mole fraction range of 0.5–0.8 and then gradually decreases with increasing mole fraction of 1*H*-1,2,4-triazole. Fig. 5b shows the TG curves of equimolar composition, $[C_2H_3N_3]/[CH_3SO_3H]$ = 75/25 composition and neat 1*H*-1,2,4-triazole with a heating rate of 1 K min^{-1}. The TG curves for the equimolar composition and 1*H*-1,2,4-triazole both show a one-step weight loss process. This is further evidence for the complete formation of 1,2,4-triazolium methanesulfonate. In contrast, the TG curve for the $[C_2H_3N_3]/[CH_3SO_3H]$ = 75/25 composition shows two weight loss events at lower and higher temperatures corresponding to the loss of excess 1*H*-1,2,4-triazole and that of 1,2,4-triazolium methanesulfonate, respectively. This also validates the powder XRD results, shown in Fig. 4, proving that no independent third phase exists in the base-rich region.

3.4 Infrared studies

FT-IR measurements were conducted to characterize the $C_2H_3N_3$–CH_3SO_3H system with an attention to the interactions between the Brønsted acid, CH_3SO_3H, and the Brønsted base, $C_2H_3N_3$. Fig. 6 shows FT-IR spectra of different compositions of the system. The very low water contents are confirmed by the absence of O–H stretching bands between 3400 and 3800 cm^{-1} in the IR spectra of the system.[16e] The IR spectra of liquid CH_3SO_3H and solid 1*H*-1,2,4-triazole are in good agreement with those reported before.[37–42] The typical absorption bands for methanesulfonic acid and 1*H*-1,2,4-triazole as well as the new bands for the equimolar composition are summarized in Table 3.

In the IR spectra of acid-rich region shown in Fig. 6, the bands related to CH_3SO_3H or $CH_3SO_3^-$ are nearly unaffected by the increase of mole fraction of 1*H*-1,2,4-triazole. Only slight weakening of some bands is observed. In the whole system, the positions of the bands associated with vibrations of the methyl group are relatively unaffected by the mole fraction changes of 1*H*-1,2,4-triazole. They appear at 771 cm^{-1} (S–C stretch), 1335 cm^{-1} (CH_3 symmetric deformation), 1416 cm^{-1} (CH_3 asymmetric deformation) and 3030 cm^{-1} (CH_3 asymmetric stretch) in the acid-rich region,[37,39] having their counterparts in the spectrum of equimolar composition at 776, 1345, 1411 and 1438,[48,49] and 3027 cm^{-1}, respectively. Conversely, the two medium intense bands at 908 cm^{-1} (S–OH stretch) and 1351 cm^{-1} (SO_2 asymmetric stretch),[37,39,43] which clearly characterize the excess acid molecules, consequently disappear in the equimolar composition and base-rich region, suggesting that there is little or no acid in them. Besides, hydrogen bonding has been identified as an important intermolecular interaction that provides structural stability to methanesulfonic acid.[39] In the present study, due to extensive hydrogen bond formation, the IR spectra of CH_3SO_3H and acid-rich region exhibit broad absorption bands at 908 cm^{-1}, 1172 cm^{-1} (O–H bend),[38,39] 1194 and 1199 cm^{-1} (SO_2 symmetric stretch),[44] and 1351 cm^{-1}, respectively. Particularly, while the absorption peak at 1254 cm^{-1} in the IR spectrum of methanesulfonic acid might be associated with asymmetric stretch of $-SO_3^-$ group,[45] the bands at 1061 and 1081 cm^{-1} most probably belong to the SO_3 symmetric stretching mode of $CH_3SO_3^-$,[43,51] which is due to the dissociation of methanesulfonic acid in ultra low water content shown in eqn (2) and (3).[46,47] This suggests that methanesulfonic acid molecules exist in associated forms (dimer) in the liquid phase. Actually, the absorption bands of the investigated methanesulfonic acid here are in line with the vibrational spectrum of methanesulfonic acid dimer observed by Durig *et al.*[39] In the acid-rich region, the reaction of 1*H*-1,2,4-triazole with acid resulting in sulfonates also contributes to the absorption bands of $CH_3SO_3^-$.

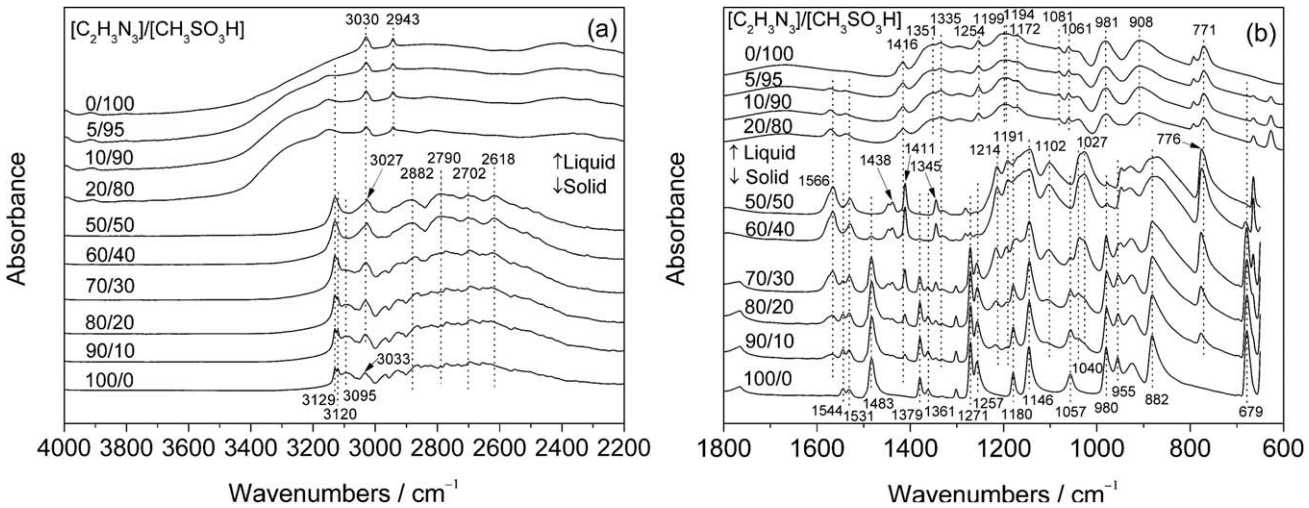

Fig. 6 FT-IR spectra of $C_2H_3N_3$–CH_3SO_3H system at room temperature in the region of 2200–4000 cm^{-1} (a) and 600–1800 cm^{-1} (b).

$$CH_3SO_3H + H_2O \leftrightarrow CH_3SO_3^- + H_3O^+ \quad (2)$$

$$2CH_3SO_3H \leftrightarrow CH_3SO_3^- + CH_3SO_3H_2^+ \quad (3)$$

In the IR spectra of the equimolar composition and base-rich region, the bands related to the SO_3 group are markedly influenced by the mole fraction of CH_3SO_3H. The intensities reach maxima at the equimolar composition, probably due to the peak concentration of $CH_3SO_3^-$ ions. Herein, the sharp absorption bands at around 1191 and 1214 cm^{-1} correspond to the SO_3 asymmetric stretching vibration of $CH_3SO_3^-$.[24,43,48] According to Langner and Zundel,[45] this spectral feature is characteristic for a $CH_3SO_3^-$ anion strongly involved in a hydrogen bond. The peaks at 1027, 1040 and 1102 cm^{-1} are most probably attributed to the SO_3 symmetric stretching vibration of $CH_3SO_3^-$.[45,48–51] Interestingly, similar to the intermolecular interactions between sulfonated bisphenol A polyetherimide and 1*H*-1,2,4-triazole,[51] hydrogen bond formation leads to broad absorption bands at 1027, 1040 cm^{-1} and 1191, 1214 cm^{-1}, with a medium strong peak at 1102 cm^{-1} associated with free sulfonate groups. As depicted in Fig. 6, the spectral changes of $CH_3SO_3^-$ ions observed with increased methanesulfonic acid content in the base-rich region are listed as follows: (i) the intensities of the SO_3 peaks at 1102, 1191 an 1214 cm^{-1} increased, (ii) the absorption bands at 1191 and 1214 cm^{-1} exhibit red shift, (iii) the peaks at 1027 and 1040 cm^{-1} gradually broaden, and (iv) the bands related to S–C stretch (776 cm^{-1}) and CH_3 deformation of $CH_3SO_3^-$ (1411 and 1345 cm^{-1}) become more and more notable.

Table 3 Typical FT-IR absorption bands of $C_2H_3N_3$–CH_3SO_3H system

Components	Wave number/cm^{-1}	Assignment	References
CH_3SO_3H	3030	CH_3 asymmetric stretch	37,39
CH_3SO_3H	2943	CH_3 symmetric stretch	37,39
CH_3SO_3H	1416	CH_3 asymmetric deformation	37,39
CH_3SO_3H	1351	SO_2 asymmetric stretch (associated)	37,39,43
CH_3SO_3H	1335	CH_3 symmetric deformation	37,39
CH_3SO_3H	1254	Asymmetric stretch of $–SO_3^-$ group	45
CH_3SO_3H	1199, 1194	SO_2 symmetric stretch	44
CH_3SO_3H	1172	O–H bend	38,39
CH_3SO_3H	1061, 1081	SO_3 symmetric stretch of $CH_3SO_3^-$	43,51
CH_3SO_3H	981	CH_3 rock	37,39
CH_3SO_3H	908	S–OH stretch (associated)	37,39,43
CH_3SO_3H	771	S–C stretch	37
1	2882, 2790, 2702, 2618	N–H or N^+–H stretch	10,42
1	1566	Protonated triazole ring stretch	56
1	1214, 1191	SO_3 asymmetric stretch of $CH_3SO_3^-$	24,43,48
1	1102, 1040, 1027	SO_3 symmetric stretch of $CH_3SO_3^-$	45,48–51
1*H*-1,2,4-Triazole	3129, 3120, 3095	C–H stretch	41,42
1*H*-1,2,4-Triazole	3200–2400	Associated N–H stretch	42
1*H*-1,2,4-Triazole	1544, 1531	C=N stretch, C–N stretch	52–55
1*H*-1,2,4-Triazole	1483, 1379, 1361, 1271, 1257, 1180, 1146, 1057	Ring stretch	41
1*H*-1,2,4-Triazole	980, 955	Ring deformation	42
1*H*-1,2,4-Triazole	924, 882	C–H out-of-plane bend	41
1*H*-1,2,4-Triazole	679	Ring torsion	52

The effects of increasing methanesulfonic acid mole fraction on the absorption bands of 1*H*-1,2,4-triazole in the base-rich and equimolar compositions can be summarized as follows: (i) the absorption peaks at 679 cm^{-1} (ring torsion),[52] 882 cm^{-1} (C–H out-of-plane bend),[41] 955 and 980 cm^{-1} (ring deformation)[42] exhibit a clear red shift with increasing mole fraction of CH_3SO_3H compared with neat 1*H*-1,2,4-triazole. The intensities of these peaks also decrease. Meanwhile, the peak at 882 cm^{-1} broadens. The band at 679 cm^{-1} splits into doublets and becomes a single peak again in the equimolar composition and the acid-rich region. As Guhathakurta and Min[51] have observed, it is the increasing interactions between 1*H*-1,2,4-triazole molecules and sulfonic acids that cause red shift of the bands characterizing triazole ring deformation and ring torsion. (ii) The bands at 1483, 1379, 1361, 1271, 1257, 1180, 1146 and 1057 cm^{-1}, which are associated with 1*H*-1,2,4-triazole ring stretch,[41] weaken, exhibit red shift or broaden, showing the protonation of 1*H*-1,2,4-triazole ring.[50,51] Particularly, the distinct peaks at 1483, 1379, 1361, 1271 and 1057 cm^{-1} are not observed in the equimolar composition, suggesting that there is no or little neat 1*H*-1,2,4-triazole in the equimolar composition. As discussed above, there is also little acid in the equimolar mixture, indicating a low concentration of methanesulfonic acid and a high content of methanesulfonate ions. These results show that the equimolar composition is clearly distinguishable from mixtures with excess acid or base, which are in line with the XRD and TGA results. In accordance with recent findings about ammonium-based protic ionic liquids,[33] such distinction in the IR spectrum of the equimolar composition from the acid-rich or base-rich compositions also led us to conclude that the equimolar composition is ionized to a high degree. (iii) Proton exchange reactions are evidenced by the decrease in the intensity of the C=N stretching peak at 1544 cm^{-1}, and correspondingly by the increase in the intensity of the C–N peak at 1531 cm^{-1}.[52–54] (iv) The intensities of the bands extending over the frequency range 3200–2400 cm^{-1}, assigned as N–H stretching vibrations,[42] increase in parallel with the increase in the acid content in the base-rich region, indicating that the N–H bonds become stronger when 1*H*-1,2,4-triazole is protonated. Furthermore, the absorption bands of equimolar composition at 2882, 2790, 2702 and 2618 cm^{-1} should be related to associated N–H stretching vibrations in the protonated 1*H*-1,2,4-triazole (*i.e.* 1,2,4-triazolium cation) compared with the spectrum of neat 1*H*-1,2,4-triazole.[42,55] The relative increase in the intensity of the N–H stretching vibration can be considered as additional evidence of salt formation.[10,54] (v) The bands at 3129 and 3120 cm^{-1} representing C–H stretch[41,42] of 1*H*-1,2,4-triazole coalesce into a single peak at 3129 cm^{-1} that still appears in the spectra of acid-rich compositions. (vi) In the region of 3200–2400 cm^{-1}, the broadening of the bands can be attributed to a hydrogen bonding network formation,[55] corroborating the findings from single crystal data of 1*H*-1,2,4-triazole[35] and 1,2,4-triazolium methanesulfonate (this work).

In addition to the new peaks corresponding to $CH_3SO_3^-$ (1214, 1191, 1102, 1040 and 1027 cm^{-1}) and N–H stretch (2882, 2790, 2702 and 2618 cm^{-1}), a new absorption band appears at 1566 cm^{-1} in the spectrum of the equimolar composition, which is attributed to the protonation of 1*H*-1,2,4-triazole.[56] It gradually weakens as the base or acid content increases, indicating that the concentration of 1,2,4-triazolium cations maximizes in the equimolar composition.

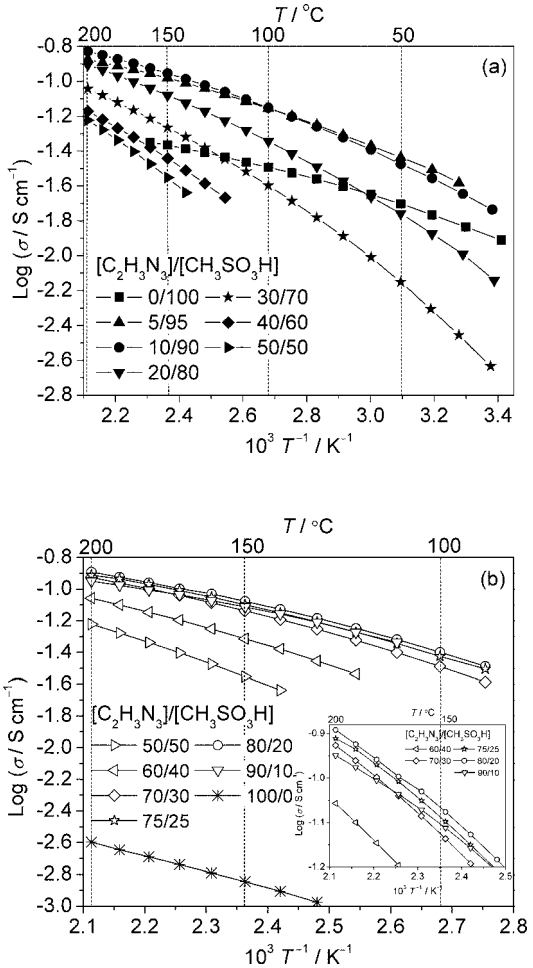

Fig. 7 Arrhenius plot for the ionic conductivity of the $C_2H_3N_3$–CH_3SO_3H system: (a) acid-rich region; (b) base-rich region (the inset shows an expanded view of the ionic conductivity for selected compositions).

FT-IR spectroscopic analysis results as well as single crystal data thus demonstrate that 1*H*-1,2,4-triazole reacts with methanesulfonic acid *via* proton transfer, producing 1,2,4-triazolium methanesulfonate, which exists in a network of strong hydrogen bonds.

3.5 Ionic conduction behavior

The ionic conductivities of the $C_2H_3N_3$–CH_3SO_3H system were studied to clarify the ionic transport behavior and the proton transfer mechanism. The temperature dependence of the ionic conductivity for the acid-rich and base-rich compositions is shown in Fig. 7a and b, respectively. Herein, the ionic conductivity of CH_3SO_3H is 12.3 mS cm^{-1} at 20 °C, which is higher than the extrapolated value of 0.59 mS cm^{-1} for anhydrous CH_3SO_3H at 25 °C.[46] The ionic conductivity of 1*H*-1,2,4-triazole is 1.06 mS cm^{-1} at 130 °C, lower than 2.1 mS cm^{-1} at 128 °C reported by Liu *et al.*,[13] probably due to the higher purity of 1*H*-1,2,4-triazole we used.

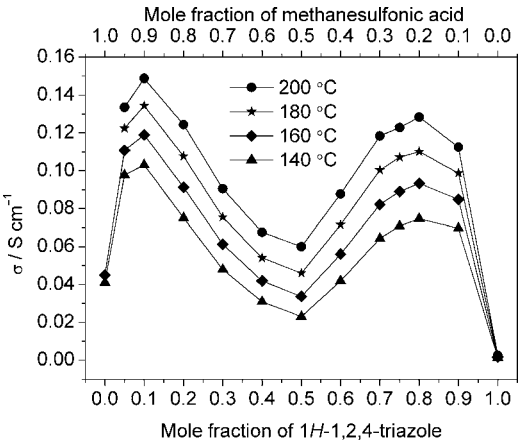

Fig. 8 Isothermal ionic conductivities for the $C_2H_3N_3$–CH_3SO_3H system as a function of 1*H*-1,2,4-triazole content.

Table 4 VFT fitting parameters for the ionic conductivity of $C_2H_3N_3$–CH_3SO_3H system

$[C_2H_3N_3]/[CH_3SO_3H]$	A/S K$^{1/2}$ cm^{-1}	B/K	T_0/K	R^{2a}
0/100[b]	4.091	409.6	155.4	0.9999
5/95	16.74	568.2	147.2	0.9999
10/90	23.87	654.8	144.4	0.9999
20/80	34.14	825.7	147.5	0.9999
30/70	35.87	897.2	164.2	0.9999
40/60	41.62	991.5	176.7	0.9999
50/50	44.09	937.8	206.8	0.9999
60/40	31.46	750.2	205.4	0.9999
70/30	25.94	608.2	209.6	0.9999
75/25	24.99	600.0	203.0	0.9997
80/20	19.81	497.0	219.8	0.9999
90/10	11.45	353.9	244.0	0.9999
100/0	1.949	1202	136.9	0.9998

[a] R^2: correlation coefficient. [b] Upper temperature limit for CH_3SO_3H was 160 °C.

The composition dependence of the isothermal ionic conductivity is presented in Fig. 8 for better interpretation. Obviously, in the acid-rich region, the ionic conductivity increases as the mole fraction of 1*H*-1,2,4-triazole decreases until it reaches a local maximum at the $[C_2H_3N_3]/[CH_3SO_3H]$ = 10/90 composition. Herein, the highest ionic conductivity at 200 °C is 0.149 S cm^{-1}. The ionic conductivity reduces notably when the mole fraction of 1*H*-1,2,4-triazole further decreases. It is minimized at the composition of pure CH_3SO_3H. In the base-rich region, the ionic conductivity of the system above the melting point increases with increasing mole fraction of 1*H*-1,2,4-triazole until it reaches another local maximum at the $[C_2H_3N_3]/[CH_3SO_3H]$ = 80/20 composition, which happens to be around the eutectic composition. At 200 °C, the peak ionic conductivity is 0.128 S cm^{-1}. When 1*H*-1,2,4-triazole content further rises, the ionic conductivity sharply decreases. Neat 1*H*-1,2,4-triazole has the lowest ionic conductivity (*e.g.* 0.00253 S cm^{-1} at 200 °C). The equimolar composition, which has the highest melting point, shows a local minimum of ionic conductivity. Overall, the composition dependence of the ionic conductivity in the $C_2H_3N_3$–CH_3SO_3H system is quite similar to the whole imidazole–sulfuric acid system,[20] the imidazole–HTFSI and 2,5-diphenyl-1,3,4-oxadiazole–HTFSI systems in the base-rich region,[10,18] and the *N*-methylpyrrolidine–acetic acid system[21] in the acid-rich region.

The Arrhenius plots depicted in Fig. 7 indicate that the ionic conductivity exhibits systematic deviation from a simple Arrhenius behavior. Therefore, the Vogel–Fulcher–Tamman (VFT) equation[57] (4) was used to analyze the ion conduction behavior. A is proportional to the concentration of carrier ions, B is the pseudo activation energy for ion conduction, and T_0 is the ideal glass transition temperature.[58,59]

$$\sigma(T) = \frac{A}{\sqrt{T}}\exp\left(\frac{-B}{T - T_0}\right) \quad (4)$$

For ionic liquids, T_0 is usually 30–60 K below the calorimetric glass transition temperature T_g.[60] However, due to the lack of T_g data for our system, T_0 was used as an adjustable fitting parameter that minimized the deviation from eqn (4).[59] The best-fit parameters were calculated for the experimental results and are listed in Table 4. These VFT plots are shown in Fig. 9. From the correlation coefficient and the straight lines depicted in Fig. 9, it is clear that the ionic conductivity of the whole $C_2H_3N_3$–CH_3SO_3H system follows the prediction of the VFT equation very well. Interestingly, the fitting results indicated that the relation between carrier ion concentration and the mole fraction of 1*H*-1,2,4-triazole exhibited a volcano shape with the equimolar composition having the most carrier ions at the top and 1*H*-1,2,4-triazole and CH_3SO_3H the least carrier ions at the bottom. It is in line with the FT-IR spectroscopic results which revealed that the concentration of 1,2,4-triazolium cations maximizes in the equimolar composition. Obviously, with the addition of acid in the base-rich region, more ions were produced and hence the ion concentration also increased. Besides, the parameter B for 1*H*-1,2,4-triazole was the highest, which also explained why 1*H*-1,2,4-triazole had the lowest ionic conductivity.

However, although the equimolar composition had the maximum concentration of carrier ions, it showed a local minimum of ionic conductivity as has been mentioned above. As the ionic conductivity of amorphous materials depends on

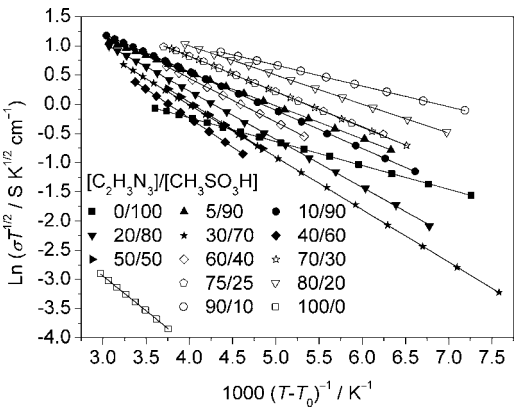

Fig. 9 VFT plots of ionic conductivities for the $C_2H_3N_3$–CH_3SO_3H system. The lines represent the VFT fittings.

both carrier ion concentration and mobility,[15c,61] the viscosity of the equimolar composition is expected to be relatively high in liquid state, leading to low ion mobilities. This has been partly indicated by the highest melting point of the equimolar composition in the system. In the base-rich region the ionic conductivity increased remarkably when 1*H*-1,2,4-triazole mole fraction from the equimolar composition was increased. The effect of reduced carrier ion concentration was over-compensated by markedly enhanced ionic mobility. As is well known, Grotthuss mechanism (intermolecular proton transfer) and vehicle mechanism (matrix transport) are two typical mechanisms of proton conduction.[62] According to Kreuer *et al.*[20] and Watanabe *et al.*,[18] the proton conduction in the imidazole–sulfuric acid system and the imidazole–HTFSI system is due not only to the vehicle mechanism but also to Grotthuss mechanism involving protonated and neat imidazole. Because of self-dissociation, proton conduction also exists in neat imidazole. Kreuer *et al.*[20] further pointed out that the imidazolium ion in imidazole-rich compositions accelerates proton transfer mainly *via* the Grotthuss mechanism. 1*H*-1,2,4-Triazole has a similar molecular structure as that of imidazole and therefore may conduct protons *via* Grotthuss mechanism. Similar to that in imidazole, Liu *et al.*[13] reported that self-dissociation of 1*H*-1,2,4-triazole produces proton charge carriers and the mobility of the proton charge carriers is very high. They discovered that proton transfer between the triazole rings makes a major contribution to the observed ionic conduction in the 1*H*-1,2,4-triazole–$C_{12}PhSO_3H$ system with 9 mol% acid.[13] Consequently, in our system the intermolecular proton transfer between the protonated 1*H*-1,2,4-triazole and neat 1*H*-1,2,4-triazole should also contribute to the ionic conductivity in the base-rich region.

On the other hand, since the ionic conductivity of the whole $C_2H_3N_3$–CH_3SO_3H system obeys the VFT equation, the vehicle mechanism should mainly govern the proton conduction in this system.[15c,63] Nakamoto and Watanabe[15b] reported that in the PIL obtained from the equimolar combination of $(C_2H_5)_2CH_3N$ and CF_3SO_3H, the dissociated active proton from CF_3SO_3H mainly diffuses as $(C_2H_5)_2CH_3HN^+$ through the vehicle mechanism. Similarly, in our equimolar composition, the dissociated proton from CH_3SO_3H should mainly transfer as 1,2,4-triazolium *via* the same mechanism.

Therefore, we conclude that the proton conduction in the base-rich region follows a combination of Grotthuss-type and vehicle-type mechanisms. However, it is still necessary to further investigate the proton conduction mechanism in the system using advanced tools like pulsed field gradient NMR technique.[19,20]

3.6 Electrochemical stability

As shown in Fig. 10, the electrochemical stability of **1**, methanesulfonic acid and 1*H*-1,2,4-triazole was investigated using a Pt micro-disk electrode at 150 °C with a scan rate of 2 mV s^{-1}. The electrochemical window (EW) displayed in Table 5 was defined as the potential range where the limiting current density reached 1.0 mA cm^{-2}. The EWs were found to be around 2.0, 1.8 and 2.1 V for **1**, CH_3SO_3H and $C_2H_3N_3$, respectively. The high electrochemical stability of 1*H*-1,2,4-triazole also agrees well with previous reports.[13,27] These wide EWs indicate that the

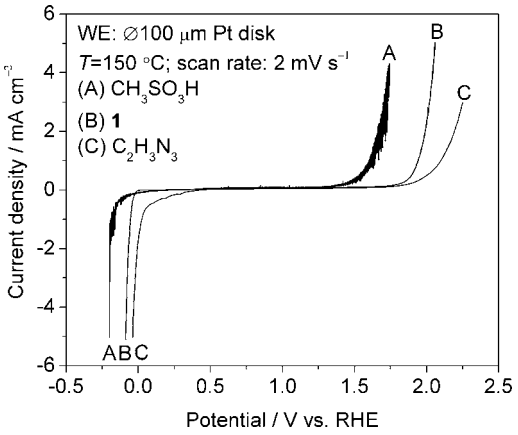

Fig. 10 Linear sweep voltammograms performed with Pt micro-disk electrode at 150 °C and a scan rate of 2 mV s^{-1}: CH_3SO_3H (A), **1** (B) and $C_2H_3N_3$ (C).

Table 5 Cathodic and anodic limits (*vs.* RHE) and electrochemical windows (EWs) at 150 °C

Composition	Cathodic limit/V	Anodic limit/V	EW/V
CH_3SO_3H	−0.16	1.62	1.8
1	−0.05	1.94	2.0
$C_2H_3N_3$	0.02	2.10	2.1

$C_2H_3N_3$–CH_3SO_3H system is electrochemically stable under PEMFC conditions and therefore could be potentially used as high temperature PEMFC electrolytes. They may also be used as non-aqueous proton-conducting electrolytes for other applications.

4 Conclusions

Results of the systematic investigation of physicochemical properties of the PIL and ionic melts prepared from methanesulfonic acid and 1*H*-1,2,4-triazole were reported. XRD characterizations indicated that the equimolar composition was **1**. The protonation of triazole rings with methanesulfonic acid was proved with single crystal XRD and FT-IR. Powder XRD and TG analysis showed that no further independent compound exists in the base-rich region. It was found that the $C_2H_3N_3$–CH_3SO_3H system exists in a network of strong hydrogen bonds. Maximum ionic conductivities of 0.149 and 0.128 S cm^{-1} at 200 °C were obtained for the acid-rich and base-rich compositions, respectively. The ionic conductivity of the system obeyed the VFT equation very well. In addition, the $C_2H_3N_3$–CH_3SO_3H system showed adequate electrochemical stability for PEMFC operations. The good thermal stability, high ionic conductivity, wide electrochemical window and simple synthesis as well as the technical availability and well documented toxicology of the starting materials make the $C_2H_3N_3$–CH_3SO_3H system a highly interesting candidate for high temperature PEMFC electrolytes under non-humidifying conditions. Further work for the development of ionic-liquid-based polymer membranes using the strategy of immobilizing ionic liquids is going to be carried out in our lab.

Acknowledgements

The authors gratefully acknowledge technical discussions with Prof. Dr Frank Endres (Technische Universität Clausthal) and Dr Jan Leys (Katholieke Universiteit Leuven). We are also deeply indebted to Dr Martin Knipper and Ms Katja Rieß (Universität Oldenburg) for their assistance with powder XRD and DTA/TGA experiments, respectively. Ivo Vankelecom wishes to thank the IOF of K. U. Leuven and IWT-SBO, respectively, for grants on ionic liquids and fuel cells.

References

1 (*a*) B. C. H. Steele and A. Heinzel, *Nature*, 2001, **414**, 345; (*b*) Q. Li, R. He, J. O. Jensen and N. J. Bjerrum, *Chem. Mater.*, 2003, **15**, 4896; (*c*) J. Zhang, Z. Xie, J. Zhang, Y. Tang, C. Song, T. Navessin, Z. Shi, D. Song, H. Wang, D. P. Wilkinson, Z. Liu and S. Holdcroft, *J. Power Sources*, 2006, **160**, 872; (*d*) R. Devanathan, *Energy Environ. Sci.*, 2008, **1**, 101.

2 (*a*) G. Alberti and M. Casciola, *Annu. Rev. Mater. Res.*, 2003, **33**, 129; (*b*) M. A. Hickner, H. Ghassemi, Y. S. Kim, B. R. Einsla and J. E. McGrath, *Chem. Rev.*, 2004, **104**, 4587; (*c*) K. A. Mauritz and R. B. Moore, *Chem. Rev.*, 2004, **104**, 4535; (*d*) K. D. Kreuer, S. J. Paddison, E. Spohr and M. Schuster, *Chem. Rev.*, 2004, **104**, 4637.

3 (*a*) Y. Sone, P. Ekdunge and D. Simonsson, *J. Electrochem. Soc.*, 1996, **143**, 1254; (*b*) T. Tago, H. Shibata and H. Nishide, *Chem. Commun.*, 2007, 2989; (*c*) J. Hu, J. Luo, P. Wagner, O. Conrad and C. Agert, *Electrochem. Commun.*, 2009, **11**, 2324.

4 W. Xu and C. A. Angell, *Science*, 2003, **302**, 422.

5 (*a*) M. Armand, F. Endres, D. R. MacFarlane, H. Ohno and B. Scrosati, *Nat. Mater.*, 2009, **8**, 621; (*b*) T. L. Greaves and C. J. Drummond, *Chem. Rev.*, 2008, **108**, 206; (*c*) D. R. MacFarlane, M. Forsyth, P. C. Howlett, J. M. Pringle, J. Sun, G. Annat, W. Neil and E. I. Izgorodina, *Acc. Chem. Res.*, 2007, **40**, 1165; (*d*) C. A. Angell, N. Byrne and J.-P. Belieres, *Acc. Chem. Res.*, 2007, **40**, 1228.

6 (*a*) H. Ye, J. Huang, J. J. Xu, N. K. A. C. Kodiweera, J. R. P. Jayakody and S. G. Greenbaum, *J. Power Sources*, 2008, **178**, 651; (*b*) A. Fernicola, S. Panero and B. Scrosati, *J. Power Sources*, 2008, **178**, 591; (*c*) A. Fernicola, S. Panero, B. Scrosati, M. Tamada and H. Ohno, *ChemPhysChem*, 2007, **8**, 1103; (*d*) A. Martinelli, A. Matic, P. Jacobsson, L. Börjesson, A. Fernicola, S. Panero, B. Scrosati and H. Ohno, *J. Phys. Chem. B*, 2007, **111**, 12462; (*e*) Q. Che, B. Sun and R. He, *Electrochim. Acta*, 2008, **53**, 4428; (*f*) W. Ogihara, J. Sun, M. Forsyth, D. R. MacFarlane, M. Yoshizawa and H. Ohno, *Electrochim. Acta*, 2004, **49**, 1797.

7 (*a*) S.-Y. Lee, A. Ogawa, M. Kanno, H. Nakamoto, T. Yasuda and M. Watanabe, *J. Am. Chem. Soc.*, 2010, **132**, 9764; (*b*) S.-Y. Lee, T. Yasuda and M. Watanabe, *J. Power Sources*, 2010, **195**, 5909.

8 (*a*) V. D. Noto, E. Negro, J.-Y. Sanchez and C. Iojoiu, *J. Am. Chem. Soc.*, 2010, **132**, 2183; (*b*) C. Iojoiu, M. Hana, Y. Molmeret, M. Martinez, L. Cointeaux, N. El Kissi, J. Teles, J.-C. Leprêtre, P. Judeinstein and J.-Y. Sanchez, *Fuel Cells*, 2010, **10**, 778; (*c*) C. Iojoiu, M. Martinez, M. Hanna, Y. Molmeret, L. Cointeaux, J.-C. Leprêtre, N. E. Kissi, J. Guindet, P. Judeinstein and J.-Y. Sanchez, *Polym. Adv. Technol.*, 2008, **19**, 1406.

9 (*a*) F. Yan, S. Yu, X. Zhang, L. Qiu, F. Chu, J. You and J. Lu, *Chem. Mater.*, 2009, **21**, 1480; (*b*) B. Lin, S. Cheng, L. Qiu, F. Yan, S. Shang and J. Lu, *Chem. Mater.*, 2010, **22**, 1807.

10 H. Matsuoka, H. Nakamoto, M. A. B. H. Susan and M. Watanabe, *Electrochim. Acta*, 2005, **50**, 4015.

11 (*a*) M. Hirao, K. Ito and H. Ohno, *Electrochim. Acta*, 2000, **45**, 1291; (*b*) M. Yoshizawa, W. Ogihara and H. Ohno, *Polym. Adv. Technol.*, 2002, **13**, 589.

12 (*a*) J. S. Wainright, J.-T. Wang, D. Weng, R. F. Savinell and M. Litt, *J. Electrochem. Soc.*, 1995, **142**, L121; (*b*) J.-T. Wang, R. F. Savinell, J. Wainright, M. Litt and H. Yu, *Electrochim. Acta*, 1996, **41**, 193; (*c*) Y. Zhai, H. Zhang, Y. Zhang and D. Xing, *J. Power Sources*, 2007, **169**, 259.

13 S. Li, Z. Zhou, Y. Zhang, M. Liu and W. Li, *Chem. Mater.*, 2005, **17**, 5884.

14 A. Aslan and A. Bozkurt, *J. Power Sources*, 2009, **191**, 442.

15 (*a*) M. A. B. H. Susan, A. Noda, S. Mitsushima and M. Watanabe, *Chem. Commun.*, 2003, 938; (*b*) H. Nakamoto and M. Watanabe, *Chem. Commun.*, 2007, 2539; (*c*) W. Ogihara, H. Kosukegawa and H. Ohno, *Chem. Commun.*, 2006, 3637; (*d*) S. Mitsushima, Y. Shinohara, K. Matsuzawa and K.-I. Ota, *Electrochim. Acta*, 2010, **55**, 6639; (*e*) T. Yasuda, A. Ogawa, M. Kanno, K. Mori, K. Sakakibara and M. Watanabe, *Chem. Lett.*, 2009, **38**, 692.

16 (*a*) J.-P. Belieres, D. Gervasio and C. A. Angell, *Chem. Commun.*, 2006, 4799; (*b*) J. Thomson, P. Dunn, L. Holmes, J.-P. Belieres, C. A. Angell and D. Gervasio, *ECS Trans.*, 2008, 21; (*c*) M. Yoshizawa, W. Xu and C. A. Angell, *J. Am. Chem. Soc.*, 2003, **125**, 15411; (*d*) J. A. Bautista-Martinez, L. Tang, J.-P. Belieres, R. Zeller, C. A. Angell and C. Friesen, *J. Phys. Chem. C*, 2009, **113**, 12586; (*e*) J.-P. Belieres and C. A. Angell, *J. Phys. Chem. B*, 2007, **111**, 4926.

17 (*a*) M. Anouti, M. Caillon-Caravanier, C. L. Floch and D. Lemordant, *J. Phys. Chem. B*, 2008, **112**, 9406; (*b*) M. Anouti, M. Caillon-Caravanier, C. L. Floch and D. Lemordant, *J. Phys. Chem. B*, 2008, **112**, 9412; (*c*) J.-F. Huang, H. Luo, C. Liang, I.-W. Sun, G. A. Baker and S. Dai, *J. Am. Chem. Soc.*, 2005, **127**, 12784; (*d*) C. Zhao, G. Burrell, A. A. J. Torriero, F. Separovic, N. F. Dunlop, D. R. MacFarlane and A. M. Bond, *J. Phys. Chem. B*, 2008, **112**, 6923.

18 A. Noda, M. A. B. H. Susan, K. Kudo, S. Mitsushima, K. Hayamizu and M. Watanabe, *J. Phys. Chem. B*, 2003, **107**, 4024.

19 H. Nakamoto, A. Noda, K. Hayamizu, S. Hayashi, H.-O. Hamaguchi and M. Watanabe, *J. Phys. Chem. C*, 2007, **111**, 1541.

20 K. D. Kreuer, A. Fuchs, M. Ise, M. Spaeth and J. Maier, *Electrochim. Acta*, 1998, **43**, 1281.

21 K. M. Johansson, E. I. Izgorodina, M. Forsyth, D. R. MacFarlane and K. R. Seddon, *Phys. Chem. Chem. Phys.*, 2008, **10**, 2972.

22 A. Schechter and R. F. Savinell, *Solid State Ionics*, 2002, **147**, 181.

23 (*a*) C. Yang, P. Costamagna, S. Srinivasan, J. Benziger and A. B. Bocarsly, *J. Power Sources*, 2001, **103**, 1; (*b*) W.-Q. Deng, V. Molinero and W. A. Goddard III, *J. Am. Chem. Soc.*, 2004, **126**, 15644.

24 A. K. Covington and R. Thompson, *J. Solution Chem.*, 1974, **3**, 603.

25 M. D. Gernon, M. Wu, T. Buszta and P. Janney, *Green Chem.*, 1999, **1**, 127.

26 K. T. Potts, *Chem. Rev.*, 1961, **61**, 87.

27 J. A. Hurd, R. Vaidhyanathan, V. Thangadurai, C. I. Ratcliffe, I. L. Moudrakovski and G. K. H. Shimizu, *Nat. Chem.*, 2009, **1**, 705.

28 C. Villagrán, M. Deetlefs, W. R. Pitner and C. Hardacre, *Anal. Chem.*, 2004, **76**, 2118.

29 G. M. Sheldrick, *Acta Crystallogr., Sect. A: Found. Crystallogr.*, 2008, **64**, 112.

30 D. R. MacFarlane, M. Forsyth, E. I. Izgorodina, A. P. Abbott, G. Annat and K. Fraser, *Phys. Chem. Chem. Phys.*, 2009, **11**, 4962.

31 J. Vila, L. M. Varela and O. Cabeza, *Electrochim. Acta*, 2007, **52**, 7413.

32 L. J. Farrugia, *J. Appl. Crystallogr.*, 1997, **30**, 565.

33 B. Nuthakki, T. L. Greaves, I. Krodkiewska, A. Weerawardena, M. I. Burgar, R. J. Mulder and C. J. Drummond, *Aust. J. Chem.*, 2007, **60**, 21.

34 P. Kölle and R. Dronskowski, *Inorg. Chem.*, 2004, **43**, 2803.

35 P. Goldstein, J. Ladell and G. Abowitz, *Acta Crystallogr., Sect. B: Struct. Crystallogr. Cryst. Chem.*, 1969, **25**, 135.

36 M. Bujak and J. Zaleski, *Z. Naturforsch., B: Chem. Sci.*, 2002, **57**, 157.

37 S. M. Chackalackal and F. E. Stafford, *J. Am. Chem. Soc.*, 1966, **88**, 4815.

38 A. Simon and H. Kriegsmann, *Chem. Ber.*, 1956, **89**, 2384.

39 J. R. Durig, L. Zhou, T. Schwartz and T. Gounev, *J. Raman Spectrosc.*, 2000, **31**, 193.

40 W. Otting, *Chem. Ber.*, 1956, **89**, 2887.

41 F. Billes, H. Endrédi and G. Keresztury, *THEOCHEM*, 2000, **530**, 183.

42 V. Ya. Grinshtein, A. A. Strazdin′ and A. K. Grinvalde, *Chem. Heterocycl. Compd.*, 1970, **6**, 231.

43 J. H. R. Clarke and L. A. Woodward, *Trans. Faraday Soc.*, 1966, **62**, 2226.

44 A. Givan, A. Loewenschuss and C. J. Nielsen, *J. Mol. Struct.*, 2005, **748**, 77.

45 R. Langner and G. Zundel, *J. Chem. Soc., Faraday Trans.*, 1998, **94**, 1805.

46 D. B. Roitman, J. McAlister and F. L. Oaks, *J. Chem. Eng. Data*, 1994, **39**, 56.
47 A. Telfah, G. Majer, K. D. Kreuer, M. Schuster and J. Maier, *Solid State Ionics*, 2010, **181**, 461.
48 M. G. Miles, G. Doyle, R. P. Cooney and R. S. Tobias, *Spectrochim. Acta, Part A*, 1969, **25**, 1515.
49 R. J. Capwell, K. H. Rhee and K. S. Seshadri, *Spectrochim. Acta, Part A*, 1968, **24**, 955.
50 Ş. Özden, S. Ü. Çelik and A. Bozkurt, *J. Polym. Sci., Part B: Polym. Phys.*, 2010, **48**, 1016.
51 S. Guhathakurta and K. Min, *Polymer*, 2009, **50**, 1034.
52 A. Chowdhury and S. T. Thynell, *Thermochim. Acta*, 2007, **466**, 1.
53 (*a*) S. Ü. Çelik, Ü. Akbey, A. Bozkurt, R. Graf and H. W. Spiess, *Macromol. Chem. Phys.*, 2008, **209**, 593; (*b*) V. Krishnakumar and R. J. Xavier, *Spectrochim. Acta, Part A*, 2004, **60**, 709.
54 F. Göktepe, A. Bozkurt and Ş. T. Günday, *Polym. Int.*, 2008, **57**, 133.
55 A. Aslan, S. Ü. Çelik, Ü. Şen, R. Haser and A. Bozkurt, *Electrochim. Acta*, 2009, **54**, 2957.
56 S. T. Günday, A. Bozkurt, W. H. Meyer and G. Wegner, *J. Polym. Sci., Part B: Polym. Phys.*, 2006, **44**, 3315.
57 (*a*) H. Vogel, *Phys. Z.*, 1921, **22**, 645; (*b*) G. S. Fulcher, *J. Am. Ceram. Soc.*, 1925, **8**, 339; (*c*) G. Tamman and W. Z. Hesse, *Z. Anorg. Allg. Chem.*, 1926, **156**, 245.
58 S. Seki, M. A. B. H. Susan, T. Kaneko, H. Tokuda, A. Noda and M. Watanabe, *J. Phys. Chem. B*, 2005, **109**, 3886.
59 H. Ohno and M. Yoshizawa, *Solid StateIonics*, 2002, **154–155**, 303.
60 H. Weingrtner, *Angew. Chem., Int. Ed.*, 2008, **47**, 654.
61 F. Endres and S. Z. E. Abedin, *Phys. Chem. Chem. Phys.*, 2006, **8**, 2101.
62 (*a*) K.-D. Kreuer, A. Rabenau and W. Weppner, *Angew. Chem., Int. Ed. Engl.*, 1982, **21**, 208; (*b*) O. F. Mohammed, D. Pines, J. Dreyer, E. Pines and E. T. J. Nibbering, *Science*, 2005, **310**, 83; (*c*) T. Ueki and M. Watanabe, *Macromolecules*, 2008, **41**, 3739.
63 M. Yoshizawa and H. Ohno, *Chem. Commun.*, 2004, 1828.

